



HAL
open science

Simulation study of discotic molecules in the vicinity of the isotropic-liquid crystal transition

Bruno Martinez-Haya, Alejandro Cuetos

► **To cite this version:**

Bruno Martinez-Haya, Alejandro Cuetos. Simulation study of discotic molecules in the vicinity of the isotropic-liquid crystal transition. *Molecular Simulation*, 2009, 35 (12-13), pp.1077-1083. 10.1080/08927020902833111 . hal-00530448

HAL Id: hal-00530448

<https://hal.science/hal-00530448>

Submitted on 29 Oct 2010

HAL is a multi-disciplinary open access archive for the deposit and dissemination of scientific research documents, whether they are published or not. The documents may come from teaching and research institutions in France or abroad, or from public or private research centers.

L'archive ouverte pluridisciplinaire **HAL**, est destinée au dépôt et à la diffusion de documents scientifiques de niveau recherche, publiés ou non, émanant des établissements d'enseignement et de recherche français ou étrangers, des laboratoires publics ou privés.

**Simulation study of discotic molecules in the vicinity
of the isotropic-liquid crystal transition**

Journal:	<i>Molecular Simulation/Journal of Experimental Nanoscience</i>
Manuscript ID:	GMOS-2008-0240.R1
Journal:	Molecular Simulation
Date Submitted by the Author:	13-Feb-2009
Complete List of Authors:	Martinez-Haya, Bruno; Universidad Pablo de Olavide, Departamento de Sistemas Fisicos, Quimicos y Naturales Cuetos, Alejandro; Universidad de Almeria, Departamento de Fisica Aplicada
Keywords:	liquid crystals, discotic molecules, stacking, Monte Carlo, equations of state

SCHOLARONE™
Manuscripts

Simulation study of discotic molecules in the vicinity of the isotropic-liquid crystal transition

Bruno Martínez-Haya *

*Departamento de Sistemas Físicos, Químicos y Naturales,
Universidad Pablo de Olavide, 41013 Seville, Spain*

Alejandro Cuetos*

Departamento de Física Aplicada, Universidad de Almería, 04020 Almería, Spain

The equilibrium and microscopic properties of systems of discotic molecules have been investigated with Monte Carlo simulations. The study focuses on the behavior of the fluid in the isotropic phase in the vicinity of the first liquid crystal transition, which involves either a nematic or a columnar phase. The molecules are modelled by rigid oblate spherocylinders with various types of interaction potentials. Molecular thickness/diameter ratios within $L/D = 0.1-0.5$ are considered. The Monte Carlo equations of state are compared with theoretical predictions for hard convex bodies, based on molecular shape and virial expansions. A good agreement is found for the hard spherocylinder system, although discrepancies arise for $L/D < 0.4$ at sufficiently large packing fraction. Particular efforts are also devoted to characterizing the formation of domains of stacked molecules in the isotropic phase for the different repulsive and attractive interaction models.

I. INTRODUCTION

Discotic molecules are at the heart of a vast number of technological applications, ranging from liquid crystals [1, 2] to nanoelectronic devices [3]. Planar disk-like molecular structures are also involved in the stacking phenomena that govern a broad class of colloidal and biochemical aggregation processes. Discotic molecules are often complex organic compounds. Remarkable efforts have been directed towards the theoretical description of stacking interactions in these systems from first principles [4], or in classical atomistic approaches [5, 6]. Due to molecular complexity, atomistic studies are computationally expensive. As a consequence, the investigation of discotic fluids demands complementary approaches, based on a coarse-grain description of the molecular structure and of the relevant interactions. Ideally,

* electronic addresses: bmarhay@upo.es, acuetos@ual.es

1 such a modelling framework should still capture the physics underlying the microscopic and mesophasic behavior of
2 discotics. The success of coarse-grain models relies in the central role that excluded volume interactions, induced by
3 molecular shape, play in colloidal behavior.
4
5
6

7 Coarse-grain studies of discotic molecules have been much more scarce than for rod-like molecules. In a recent
8 work, we have introduced an efficient methodology of general application for discotics [7]. Our approach is based
9 on the use of Kihara-type pair potentials to represent the particles as rigid discotic spherocylinders. This particle
10 geometry (a flat cylindrical core with a toroidal rim) is represented in Fig. 1. Discotic spherocylinders can be expected
11 to resemble more closely the effective shape of rigid discotic mesogens than, for instance, ellipsoidal models [8].
12
13
14

15 We report here on a study of discotic Kihara models with thickness/diameter ratios within $L^* \equiv L/D = 0.1-0.5$.
16 Computational and theoretical studies for this family of molecular fluids have been restricted thus far to the hard
17 spherocylinder fluid (OHSC). Furthermore, most previous works have been limited to the isotropic phase of particles
18 with a moderate anisotropy ($L^* > 0.3$) [10–17]. Only very recently a detailed account of different columnar phases
19 displayed by the OHSC fluid has been reported from Monte Carlo simulations [7]. This latter study demonstrated
20 that the discotic spherocylinder molecular shape intrinsically favors columnar stacking, as opposed to hard discotic
21 ellipsoids of revolution, which lack columnar phases, unless specific energetics are incorporated [8, 9].
22
23
24
25
26
27
28
29
30

31 In the present study, we consider four different types of pair interaction potentials. On one hand, hard and soft
32 repulsive spherocylinders are investigated. Furthermore, spherocylinders with soft attractive interactions around the
33 molecular core are considered. *Ab initio* computations for planar polyaromatics have shown that pair interactions
34 depend strongly on the relative orientation of the particles, even if the shortest distance between the molecular cores
35 remains unchanged [4]. Correspondingly, we have incorporated attractive interactions with an explicit dependence on
36 pair orientation into our coarse-grain model. In order to achieve this, we have followed an approach applied previously
37 to rod-like Kihara particles [18–21]. Within this framework, it is possible to build interaction potentials resembling
38 the features exposed by the *ab initio* computations on planar and dendritic molecular systems [4]. In particular, it
39 allows to mimic the interactions in graphene sheets, including systems with localized active sites.
40
41
42
43
44
45
46
47
48

49 Our colleague J.A. Mejías was intensively involved in the understanding of molecular processes on soots, a partic-
50 ularly important class of graphene networks with active sites [22, 23]. As a modest tribute to his memory, we pursue
51 the development of coarse-grain models with specific interactions, that may serve to establish effective links between
52 Statistical Mechanics and Quantum Chemistry for such systems.
53
54
55

56 This paper focuses on the behavior of the model discotics in the isotropic phase, beginning at the transition from the
57
58
59
60

liquid crystal phase with which it coexists. After describing the interaction models in Sect II, the equations of state are presented and compared with the prediction of previous theoretical approaches. Finally, one main microscopic feature of the Kihara discotics is discussed, namely, the propensity to form domains of stacked particles in the isotropic phase. Future work in our group will extend the study to determine the role of specific pair interactions on aggregation phenomena, and on the mesogenic properties of these fluids.

II. METHODOLOGY

A. Spherocylinder particle geometry

Fig.1 depicts the molecular shape of the discotic Kihara models. The surface of a hard discotic spherocylinder corresponds to the ensemble of points that are at a distance $L/2$ from an infinitely thin disk of diameter σ . The total diameter of the particle is then given by $D = \sigma + L$, and its thickness/diameter aspect ratio by $L^* = L/D$. Particles with greater values of L^* have a less planar, more spherical shape. The present study includes molecules with constant σ , and variable aspect ratios within $L^* = 0.1-0.5$. Note then that the increase of L^* involves an increment in the molecular volume (see Eq. 1).

We will compare the present simulation results for the equation of state (EOS) of the hard discotic spherocylinder fluid with predictions for hard convex bodies, based on molecular shape and virial expansions [24, 25]. Barrio and Solana [24] proposed a scaling of the Carnahan–Starling EOS to predict the behavior of convex bodies. A single scaling factor was used, namely the nonsphericity factor $\alpha = r_m s_m / (3v_m)$, which includes three basic parameters describing the molecular geometry: the volume (v_m), the surface area (s_m) and the mean curvature integral ($4\pi r_m$). Boublik [25] developed a third order virial expansion including a more involved combination of the same parameters. For hard oblate spherocylinders, these geometric parameters are given by the following expressions[11]:

$$v_m/D^3 = \frac{\pi L^{*3}}{6} + \frac{\pi^2(1-L^*)L^{*2}}{8} + \frac{\pi(1-L^*)^2 L^*}{4} \quad (1)$$

$$s_m/D^2 = \pi L^{*2} + \frac{\pi^2(1-L^*)L^*}{2} + \frac{\pi(1-L^*)^2}{2} \quad (2)$$

$$r_m/D = \frac{L^*}{2} + \frac{\pi(1-L^*)}{8} \quad (3)$$

B. Pair interaction models

We will consider four types of discotic interaction models, namely the oblate versions of the hard spherocylinder model (OHSC), the soft repulsive spherocylinder model (OSRS), the 12–6 Kihara model (OKIH), and the recently introduced Gay–Berne–Kihara model (OGBK) [20, 21]. This latter model incorporates an explicit dependence of the dispersive interactions on pair orientation, as shown in Fig.1 and described below. For spherocylinder particles, the pair interaction energy is directly related to the shortest distance between the central disks of the molecular cores, $d_m(\mathbf{r}_{ij}, \hat{\mathbf{u}}_i, \hat{\mathbf{u}}_j)$. Such distance is a complex (not analytical) function of the center-of-mass intermolecular distance vector \mathbf{r}_{ij} , and of the relative orientations of the pair of particles, defined by the directors $(\hat{\mathbf{u}}_i, \hat{\mathbf{u}}_j)$. A general description of the numerical algorithm employed to compute d_m can be found in ref. [7].

The above mentioned interactions models are defined by the following expressions.

Hard Spherocylinder potential:

$$U_{OHSC}(d_m) = \begin{cases} \infty & d_m \leq L \\ 0 & d_m > L \end{cases} \quad (4)$$

12–6 Kihara potential:

$$U_{OKIH}(d_m) = 4\epsilon \left[(\sigma/d_m)^{12} - (\sigma/d_m)^6 \right] \quad (5)$$

Soft Repulsive Spherocylinder potential:

$$U_{OSRS}(d_m) = \begin{cases} 4\epsilon \left[(\sigma/d_m)^{12} - (\sigma/d_m)^6 + 1/4 \right] & d_m \leq \sqrt[6]{2} L \\ 0 & d_m > \sqrt[6]{2} L \end{cases} \quad (6)$$

Gay–Berne–Kihara potential:

$$U_{OGBK}(\mathbf{r}_{ij}, \hat{\mathbf{u}}_i, \hat{\mathbf{u}}_j) = \epsilon_{OGB}(\hat{\mathbf{r}}_{ij}, \hat{\mathbf{u}}_i, \hat{\mathbf{u}}_j) U_{OKIH}(d_m) \quad (7)$$

$$\epsilon_{OGB}(\hat{\mathbf{r}}_{ij}, \hat{\mathbf{u}}_i, \hat{\mathbf{u}}_j) = \epsilon'_{GO}(\hat{\mathbf{u}}_i, \hat{\mathbf{u}}_j) \epsilon'^{\mu}(\hat{\mathbf{r}}_{ij}, \hat{\mathbf{u}}_i, \hat{\mathbf{u}}_j) \quad (8)$$

$$\epsilon'_{GO}(\hat{\mathbf{u}}_i, \hat{\mathbf{u}}_j) = [1 - \chi^2(\hat{\mathbf{u}}_i \cdot \hat{\mathbf{u}}_j)^2]^{-1/2} \quad (9)$$

$$\epsilon'(\hat{\mathbf{r}}_{ij}, \hat{\mathbf{u}}_i, \hat{\mathbf{u}}_j) = \mathbf{1} - \frac{\chi'}{2} \left[\frac{(\hat{\mathbf{r}}_{ij} \cdot \hat{\mathbf{u}}_i + \hat{\mathbf{r}}_{ij} \cdot \hat{\mathbf{u}}_j)^2}{1 + \chi' \hat{\mathbf{u}}_i \cdot \hat{\mathbf{u}}_j} + \frac{(\hat{\mathbf{r}}_{ij} \cdot \hat{\mathbf{u}}_i - \hat{\mathbf{r}}_{ij} \cdot \hat{\mathbf{u}}_j)^2}{1 - \chi' \hat{\mathbf{u}}_i \cdot \hat{\mathbf{u}}_j} \right] \quad (10)$$

It can be noted that the OSRS interaction potential follows from the upward shift (by the well depth ϵ) of the 12–6 Kihara potential and its truncation at the well minimum $d_{min} = \sqrt[6]{2}L$. In this way, a continuous and derivable

1 purely repulsive interaction potential energy functional is obtained. The OGBK interaction energy functional is built
 2 by multiplying the 12–6 Kihara potential by the orientational pre-factor of the discotic Gay–Berne potential [8]. All
 3 the soft potentials were truncated at $d_m = 3L$, and shifted as to make the potential continuous.
 4
 5
 6

7 Note that the Gay–Berne factor, ϵ_{OGB} is characterized by the aspect ratio L^* (often denoted κ) and the three
 8 parameters (κ', ν, μ) , with the notation $\chi = (L^{*2} - 1)/(L^{*2} + 1)$ and $\chi' = (\kappa'^{-1/\mu} - 1)/(\kappa'^{-1/\mu} + 1)$. The choice of κ' ,
 9 ν, μ is not straightforward, especially when comparing with real systems. In this context, interaction energies obtained
 10 from *ab initio* computational approaches become particularly useful. For the present study, we have employed the
 11 set of parameters $\kappa' = 5, \nu = 2$ and $\mu = 1$, as it provided a reasonable representation of the *ab initio* data of Truhlar
 12 and coworkers for pericondensed polyaromatics [4]. As illustrated by the contour plot of Fig. 1, this parametrization
 13 provides favourable energetics for stacking. For instance, for a pair of parallel particles, ϵ_{OGB} , is $\kappa'^{1/\mu} = 5$ times
 14 greater for a stacked configuration than for particles with rim–to–rim contact.
 15
 16
 17
 18
 19
 20
 21
 22
 23
 24
 25

26 C. Monte Carlo method

27
 28 Isothermal–isobaric ensemble Monte Carlo (NPT–MC) simulations were carried out following the procedure de-
 29 scribed in ref. [7]. For each value of L^* , the system was initially equilibrated in a state within the interdigitated
 30 hexatic columnar phase [7]. The fluid was subsequently melted through the different columnar and, possibly, nematic
 31 phases, to the isotropic phase. For the soft models, equilibration typically involved $2 \cdot 10^5$ MC cycles (up to $5 \cdot 10^5$ for
 32 the boundary states of the transitions), while ensemble averages scoped over $5 \cdot 10^4$ cycles. For the OHSC model, which
 33 is faster to run than the soft models, 10^6 and 10^5 cycles were applied for equilibration and averaging, respectively.
 34 The size of the systems (number of particles) used in the simulation for each model is indicated in Table I.
 35
 36
 37
 38
 39
 40
 41

42 The melting of the OHSC fluid was induced by the reduction of the pressure/temperature ratio $P^* = PD^3/k_B T$
 43 (where k_B denotes the Boltzmann constant). For the soft interaction models, OSRS, OKIH and OGBK, the melting
 44 of the liquid crystal was actually performed by increasing the temperature $T^\dagger = k_B T/\epsilon$, at constant pressure $P^\dagger =$
 45 $PD^3/\epsilon = 100$ (note that $P^* = P^\dagger/T^\dagger$). The phase transitions were characterized by discontinuities in density, energy,
 46 bond order and nematic order parameters, and by monitoring specific pair correlation functions [7].
 47
 48
 49
 50
 51

52 A detailed account of the nematic and columnar phases displayed by the different soft models will be provided
 53 elsewhere. Here, we concentrate mainly on characterizing the isotropic phase and only limited analysis of the liquid
 54 crystalline behaviour. Nevertheless, the average nematic order parameters at the different transitions are provided in
 55 Table I. The nematic phase can be easily discerned from any of the columnar phases from the lack of correlations in
 56
 57
 58
 59
 60

the distribution function along the directions parallel and perpendicular to the nematic director.

III. RESULTS

Figs. 2 and 3 show the Monte Carlo equations of state of the OHSC fluids with the five aspect ratios considered in our study. These Figures depict the isotropic branch of the fluid, from the boundary state where the transition from a liquid crystal phase takes place. Table I lists relevant parameters of the boundary states at each of the transitions and indicates the type of liquid crystal phase involved. For the OHSC fluid the transition takes place to a nematic phase (N) for $L^*=0.1$, and to three columnar phases, namely D_{hi} for $L^*=0.5$, D_{ho} for $L^*=0.4$ and D_{hd} for $L^*=0.3$ and 0.2 . Here, D_{hi} denotes a hexatic interdigitated columnar phase, D_{ho} a hexatic ordered columnar phase, and D_{hd} a hexatic disordered columnar phase, in which the columns become fluid-like [7]. Hence, the internal order of the lowest columnar phase is reduced as the molecular anisotropy is enhanced (*i.e.*, L^* becomes smaller), until the nematic phase eventually becomes stable for $L^*=0.1$. It is interesting to notice that the columnar transition shifts to smaller packing fractions as the molecules become thinner, and that the nematic transition for $L^*=0.1$ occurs at a relatively small packing fraction of the fluid.

Two different representations of the EOS are shown in Figs. 2 and 3 in order to provide a direct comparison with the analogous results for the soft particles discussed below. On one hand, the EOS are shown confronting the reduced pressure P^* with the packing fraction of the fluid, $\eta = \rho v_m$. On the other hand, the compressibility factor, $Z = \beta P / \rho = P^* / \rho^*$ is plotted against the reduced number density $\rho^* = \rho D^3$. In both representations, the EOS predicted for the OHSC fluid by the theories of refs. [24] and [25] are shown for comparison. Simulation data obtained for the nematic phase of the $L^*=0.1$ OHSC fluid are also included in Fig. 2 for reference. It can be noted that the maximum packing fraction achieved by the fluid in the isotropic phase increases with growing L^* . This follows from the greater excluded volume induced by the thinner particles, in comparison to their molecular volume, under conditions of random orientation. Similar considerations, together with the increase in molecular volume with growing particle thickness (at constant σ , see Eq. 1), explain the larger compressibility factors achieved for the fluids with larger L^* (Fig. 2). It can be observed that both theoretical EOSs reproduce very well the simulation data for the OHSC fluids with $L^* > 0.3$. At $L^*=0.3$ and smaller aspect ratios, appreciable differences appear in the immediate vicinity of the liquid crystal transition. Nevertheless, the performance of the relatively simple theories is remarkable, provided that they were developed having as reference fluids of molecules closer to sphericity ($L^* \geq 0.4$).

Figs. 4 and 5 show the EOS obtained in our simulation of the different soft oblate Kihara particles described above.

1 Fluids with $L^*=0.2$ and 0.4 are considered in this case. For soft particles, molecular volume is not well defined,
 2 and only the Z vs ρ representation is presented. We recall that the Monte Carlo simulation of the soft particle fluids
 3 was performed at constant pressure ($P^\dagger = 100$), so that the expansion of the fluid follows from sequential heating
 4 (see Sect. II). Changes in pressure led to qualitatively similar EOSs, with consistent changes in density. It can be
 5 observed that the purely repulsive potential of the OSRS fluid and also the homogeneous attractive well of the KIH
 6 fluid, both lead to a behavior qualitatively similar to that of the OHSC fluid. The isotropic EOS proceeds smoothly
 7 up to relatively high number densities before entering the domain of liquid crystalline behavior. The liquid crystal
 8 transitions in the OSRS and OKIH fluids are similar to their OHSC counterparts, namely $I-D_{ho}$ for $L^*=0.4$ and
 9 $I-D_{hd}$ for $L^*=0.2$, and occur at not too dissimilar values of Z and ρ^* .

10 In the OGBK model, the specific energetics leads to a significant shift of the liquid phase transition to lower
 11 pressures and densities. For the two aspect ratios investigated, $L^*=0.4$ and $L^*=0.2$, the OGBK EOS runs at low
 12 density close to those of the other soft models. However, the OGBK values of Z , P^* and ρ^* at the transition are
 13 appreciably smaller than those for the OHSC, OSRS and OKIH fluids. The comparison of these four models allows
 14 us to discern between the steric and the energetic contributions to the free energy responsible for mesogenic behavior
 15 in discotic liquid crystals. Table I shows that an appreciable change in internal energy takes place at the isotropic-
 16 columnar transitions of the OGBK fluids. The energy discontinuity is much smaller for the OSRS, and even for the
 17 OKIH fluids.

18 A deeper insight into the mesogenic propensity of the Kihara discotic fluids can be grasped from the microscopic
 19 structure displayed in the proximity of the liquid crystal transition. Fig. 6 shows a selection of radial distribution
 20 functions, $g(r)$, for the OHSC, OSRS, OKIH and OGBK fluids with $L^*=0.2$. For each fluid, the $g(r)$ is shown
 21 for the isotropic boundary state of the transition, and at states with densities roughly 85 and 65 percent of the
 22 boundary state density. All distributions show little structure for pair distances greater than the diameter of the
 23 molecular core ($r/D > 1$). At $r/D \approx 1$ a differentiated peak is observed which corresponds to the side-to-side rim
 24 contact distance of two parallel discotic spherocylinders. Note that the volume excluded to other particles by a freely
 25 rotating spherocylinder in a diluted phase tends to be similar to that of a sphere of its same diameter. Hence, a peak
 26 in the pair distribution at $r \approx D$ is indeed expected. Furthermore, it can be observed that this peak persist at low
 27 densities. Similarly, a less prominent but also persistent peak is observed at $r/D \approx 0.5 + L^*$, in this case associated to
 28 a T-shape type pair configuration. More interestingly, a marked peak arises in the vicinity of the phase transition
 29 at $r/D \approx L^*$. This peak is associated with the formation of domains of stacked particles in the isotropic phase. Such
 30

1 stacking domains remain relevant down to densities roughly a factor of 0.7 smaller than that of the boundary state
2
3
4 at the liquid crystal transition.

5 Efficient stacking is observed for all potential energy models, including the purely repulsive OHSC and OSRS fluids.
6
7 This indicates that stacking can be induced alone from steric interactions induced by the spherocylinder shape of the
8
9 particles. The specific attractive interactions of the OGBK model further enhance the presence of the stacked domains
10
11 due to the favorable energetics. In order to appreciate this fact, it should be noted that the distribution functions for
12
13 the OGBK fluid in Fig.6 correspond to states of smaller density than for the rest of the models. A relevant finding is
14
15 that for the OGBK fluid, the transition to the columnar phase occurs before extensive short-range stacking can take
16
17 place in the isotropic phase. This behavior illustrates how mesoscopic aggregation may be rapidly seeded by local
18
19 molecular organization under favorable energetics. On the contrary, the OHSC, OSRS and OKIH fluids allow for a
20
21 significant degree of short-range organization before entering the mesoscopic domain.
22
23
24

25 IV. SUMMARY AND CONCLUSIONS

26
27
28 We have presented a simulation study of discotic spherocylinder fluids over a broad range of thickness/diameter
29
30 ratios $L^* = 0.1-0.5$. In particular, equations of state for fluids with $L^* < 0.3$ are presented for the first time by making
31
32 use of a shortest distance algorithm reported recently [7]. In addition, four different types of interaction potentials
33
34 have been considered: a hard (OHSC) and a soft (OSRS) purely repulsive models, a model with a Lennard-Jones
35
36 attractive potential homogeneously distributed around the molecular core (OKIH) and an attractive potential with
37
38 an explicit dependence on pair orientation adjusted to favour stacked configurations (OGBK).
39

40 We find a remarkable overall agreement between the EOSs obtained by simulation for the OHSC fluid, and the pre-
41
42 diction of relatively simple theories. The theoretical EOSs reproduce closely the simulation data for $L^* > 0.3$, whereas
43
44 at smaller aspect ratios, appreciable differences appear in the immediate vicinity of the liquid crystal transition. The
45
46 soft OSRS and OKIH fluids follow a similar qualitative behaviour as the OHSC fluid along the isotropic branch, as
47
48 well as for the location and nature of the columnar transition. For the OGBK model, in contrast, the enhanced
49
50 stacking interactions lead to a significant anticipation of the liquid crystal transition.
51

52 Inspection of the radial distribution function reveals that short-range stacking domains are present in the isotropic
53
54 phase of the four model fluids, even at densities significantly lower than that of the columnar transition. A conclusion is
55
56 that the discotic spherocylinder geometry favors stacking without the need for attractive interactions. The favourable
57
58 energetics of the OGBK model does enhance the appearance of the stacked domains, but it also prompts the columnar
59
60

1 transition. On the contrary, the OHSC, OSRS and OKIH fluids allow for a more extensive local stacking in a stable
2 isotropic phase. Such behavior should be useful to model the potential of local stacking to seed clustering and
3 coagulation processes in colloidal and biomolecular systems. The formation of stacked domains in the isotropic
4 phase should also be of relevance for dynamic energy and charge transfer processes, which often demand directional
5 short-range correlations.
6
7
8
9
10

11 Acknowledgements

12 Funding is acknowledged from the Regional Government of Andalusia (projects P06-FQM-01869 and P07-FQM-
13 02600), and from the Ministry of Science and Innovation of Spain (project ENE2007-68040-C03-01, and the *Juan de*
14 *la Cierva* fellowship held by A.C.).
15
16
17
18
19
20
21
22

-
- 23
24
25 [1] S. Chandrasekhar in Handbook of Liquid Crystals, Vol. 2B (Eds.: D. Demus, J. Goodby, G. W. Gray, H.-W. Spiess, V.
26 Vill), Wiley-VCH, Weinheim, 1998, pp.749
27
28 [2] R.J. Bushby and O.R. Lozman, Curr. Opin. Coll. Interface Sci., **7**, 343 (2002)
29
30 [3] J. Wu, W. Pisula and K. Müllen, Chem. Rev. **107**, 718 (2007)
31
32 [4] Y. Zhao and D.G. Truhlar, J. Phys. Chem. C **112**, 4061 (2008)
33
34 [5] D. Andrienko, V. Marcon and K. Kremer, J. Chem. Phys. **125** 124902 (2006)
35
36 [6] P.L. Cristinziano and F. Lelj, J. Chem. Phys. **127**, 134506 (2007)
37
38 [7] A. Cuetos and B. Martínez-Haya, J. Chem. Phys., **129**, 214706 (2008)
39
40 [8] M.A. Bates and G. R. Luckhurst, J. Chem. Phys. **104**, 6696 (1996)
41
42 [9] E.M. Del Río, A. Galindo, E. de Miguel, Phys Rev. E **72**, 051707 (2005)
43
44 [10] M. Wojcik and K. E. Gubbins, Mol. Phys. **53**, 397 (1984)
45
46 [11] T. Boublik and I. Nezbeda, Coll. Czes. Chem. Commun. **51**, 2301 (1986)
47
48 [12] W. R. Cooney, S. M. Thompson and K. E. Gubbins, Mol. Phys. **66**, 1269 (1989)
49
50 [13] J. Sedlbauer, S. Labik, A. Malijevisky, Phys. Rev. E **49**, 3179 (1994)
51
52 [14] P. Kadlec, J. Janecek and T. Boublik, Mol. Phys. **98**, 473 (2000)
53
54 [15] M. J. Maeso, J. R. Solana and J. Amoros, Mat. Chem. Phys. **33**, 134 (1993)
55
56 [16] B. Mulder, Mol. Phys. **103**, 1411 (2005)
57
58 [17] F. Gámez, S. Lago, B. Garzón, P.J. Merkling and C. Vega, Mol. Phys. **106**,1331 (2008)
59
60 [18] A. Cuetos, B. Martínez-Haya, S. Lago, L. F. Rull, J. Chem. Phys. **117**, 2934 (2002)

- 1
2 [19] A. Cuetos, B. Martínez-Haya, S. Lago, L. F. Rull, Phys. Rev. E **68**, 011704 (2003)
3
4 [20] B. Martínez-Haya, A. Cuetos, S. Lago, and L. F. Rull, J. Chem. Phys. **122**, 024908 (2005)
5
6 [21] B. Martínez-Haya and A. Cuetos, J. Phys. Chem. B **111**, 8150 (2007)
7
8 [22] S. Hamad, J.A. Mejías, S. Lago, S. Picaud and P.N.M. Hoang, J. Phys. Chem. B **108**, 5405 (2004)
9
10 [23] S. Picaud, P.N.M. Hoang, S. Hamad, J.A. Mejías and S. Lago, J. Phys. Chem. B **108**, 5410 (2004)
11
12 [24] C. Barrio and J.R. Solana , J. Chem. Phys. **111**, 4640 (1999)
13
14 [25] T. Boublik, Mol. Phys. **83**, 1285 (1994)
15
16
17
18
19
20
21
22
23
24
25
26
27
28
29
30
31
32
33
34
35
36
37
38
39
40
41
42
43
44
45
46
47
48
49
50
51
52
53
54
55
56
57
58
59
60

For Peer Review Only

TABLE I: Boundary states for the isotropic–liquid crystal transitions of the model fluids studied in this work. N_p , $P^* = PD^3/k_B T$, $\eta = \rho v_m$, $\rho^* = \rho D^3$, $U^* = U/\epsilon$ and P_2 represent number of particles in the simulation, pressure/temperature ratio, packing fraction, number density, energy per particle in reduced units and nematic order parameter, respectively. The packing fraction is given for comparison with previous studies of the OHSC fluid and is computed with the molecular volume (v_m) of a OHSC particle for each given L^* [7]. The values in brackets denote the statistical uncertainty (one standard deviation) in the last digit. The last column indicates the type of liquid crystalline phase associated to the transition [7]. For the soft interaction models (OSRS, OKIH and OGBK), the simulations were performed at constant pressure $P^\dagger = PD^3/\epsilon = 100$. The transition temperatures are thus given by $T^\dagger = k_B T/\epsilon = P^\dagger/P^*$.

Model Fluid	N_p	Isotropic Phase					Liquid Crystal Phase					Phase Type
		P^*	η	ρ^*	U^*	P_2	P^*	η	ρ^*	U^*	P_2	
OHSC $L^*=0.1$	3840	31	0.305(2)	3.87(3)	-	0.03(1)	32	0.291(2)	4.07(3)	-	0.499(5)	N
OHSC $L^*=0.2$	2016	49	0.475(1)	3.29(1)	-	0.04(1)	50	0.544(1)	3.77(2)	-	0.901(4)	D_{hd}
OHSC $L^*=0.3$	2016	45	0.514(2)	2.48(1)	-	0.03(1)	46	0.577(3)	2.78(3)	-	0.842(8)	D_{hd}
OHSC $L^*=0.4$	3024	42	0.541(2)	2.04(1)	-	0.04(1)	43	0.602(1)	2.27(2)	-	0.853(3)	D_{ho}
OHSC $L^*=0.5$	1680	40	0.561(1)	1.77(1)	-	0.02(1)	41	0.611(2)	1.92(2)	-	0.852(5)	D_{hi}
OSRS $L^*=0.2$	3000	50.0	0.490(1)	3.40(1)	1.39(3)	0.04(1)	51.3	0.548(2)	3.80(1)	1.31(3)	0.856(5)	D_{hd}
OSRS $L^*=0.4$	3024	45.5	0.576(1)	2.17(1)	3.31(5)	0.02(1)	46.5	0.634(1)	2.39(1)	3.05(5)	0.842(4)	D_{ho}
OKIH $L^*=0.2$	3000	46.5	0.503(1)	3.49(1)	-2.47(4)	0.03(1)	47.6	0.584(2)	4.05(1)	-2.85(4)	0.879(5)	D_{hd}
OKIH $L^*=0.4$	3024	38.5	0.576(1)	2.17(1)	-1.79(5)	0.02(1)	39.2	0.638(2)	2.41(1)	-2.56(6)	0.820(6)	D_{ho}
OGBK $L^*=0.2$	3000	12.7	0.339(2)	2.35(1)	-9.0(1)	0.03(1)	12.8	0.519(4)	3.60(3)	-37.0(6)	0.955(2)	D_{hd}
OGBK $L^*=0.4$	3024	21.5	0.507(1)	1.91(1)	-6.6(1)	0.02(1)	21.7	0.558(2)	2.11(1)	-13.6(2)	0.84(1)	D_{ho}

FIGURE CAPTIONS

Figure 1: Representation of an oblate spherocylinder. left: top view; right: side views for the hard OHSC model (Eq. 4) and for the soft OGKB model with orientational dependent interactions (Eq. 7)).

Figure 2: Equations of State in the isotropic phase (I) for OHSC fluids with thickness/diameter aspect ratios $L^* = 0.1-0.5$. The reduced Pressure $P^* = PD^3/k_B T$ is represented against the packing fraction of the fluid η . Symbols denote Monte Carlo simulation data. Lines represent the theoretical predictions of Barrio and Solana [24] and

1
2 Boublik [25]. For $L^*=0.1$, the simulation results for the nematic branch (N) are also shown (open symbols).
3
4

5 **Figure 3:** Compressibility factor $Z=P^*/\rho^*$ versus reduced density $\rho^*=\rho D^3$ representation of the same isotropic
6 phase equations of state shown in Fig. 1.
7
8

9
10 **Figure 4:** Monte Carlo compressibility factor $Z=P^*/\rho^*$ versus reduced density $\rho^*=\rho D^3$ representation of the
11 isotropic phase equations of state of the hard and soft discotic potential models considered in this work with $L^*=0.2$.
12 The theoretical OHSC EOS from ref. [24] is also included for reference (solid line).
13
14
15

16 **Figure 5:** Same as Fig. 4 for the hard and soft discotic potential models with $L^*=0.4$. The theoretical OHSC
17 EOS from ref. [24] is also included for reference (solid line).
18
19
20

21 **Figure 6:** Radial distribution functions, $g(r)$, for the OHSC, OSRS, OKIH and OGBK fluids with $L^*=0.2$.
22 For each fluid, the $g(r)$ is shown for the isotropic boundary state (solid line) of the transition, and at states with
23 densities roughly 85, and 65 percent of the boundary state density (dashed line and dot-dashed line, respectively).
24 The pronounced peaks at $r/D \approx L^*$ are indicative of local stacking of the particles.
25
26
27
28
29
30
31
32
33
34
35
36
37
38
39
40
41
42
43
44
45
46
47
48
49
50
51
52
53
54
55
56
57
58
59
60

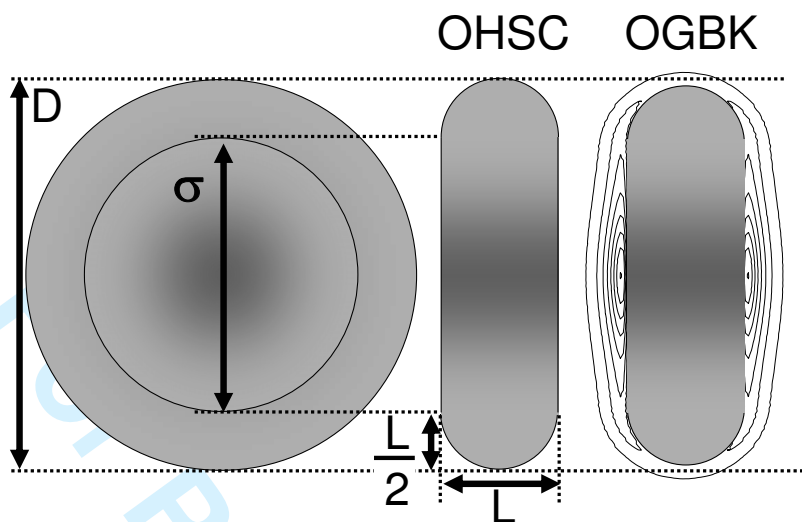


FIG. 1: Representation of an oblate spherocylinder. left: top view; right: side views for the hard OHSC model (Eq. 4) and for the soft OGBK model with orientational dependent interactions (Eq. 7).

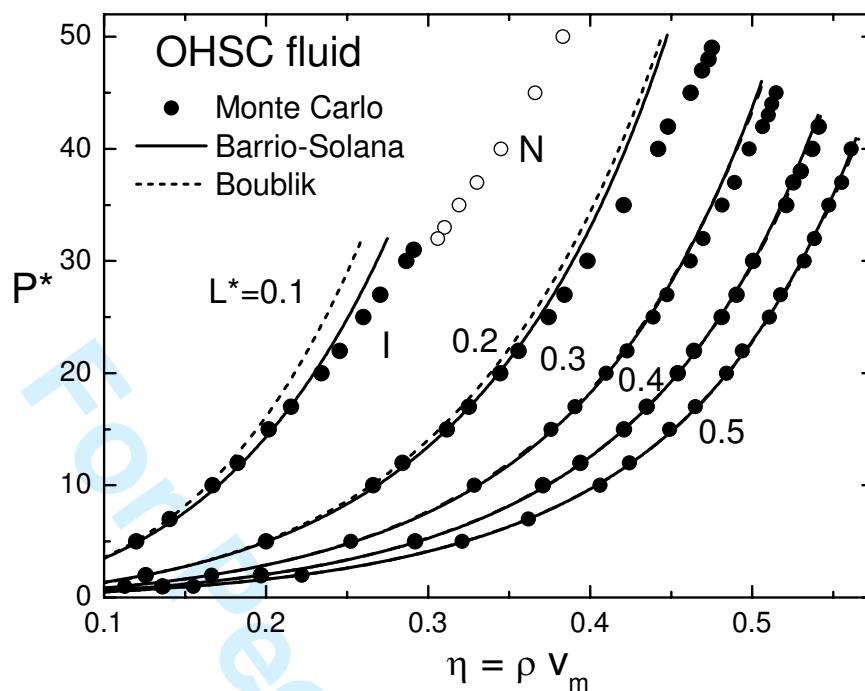


FIG. 2: Equations of State in the isotropic phase (I) for OHSC fluids with thickness/diameter aspect ratios $L^*=0.1-0.5$. The reduced Pressure $P^*=PD^3/k_B T$ is represented against the packing fraction of the fluid η . Symbols denote Monte Carlo simulation data. Lines represent the theoretical predictions of Barrio and Solana [24] and Boublik [25]. For $L^*=0.1$, the simulation results for the nematic branch (N) are also shown (open symbols).

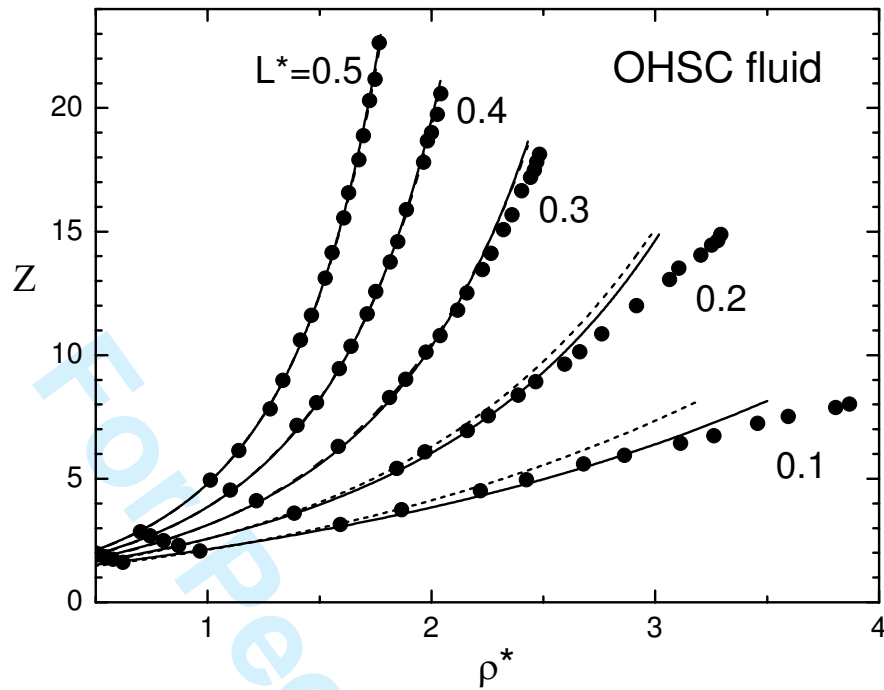


FIG. 3: Compressibility factor $Z = P^*/\rho^*$ versus reduced density $\rho^* = \rho D^3$ representation of the same isotropic phase equations of state shown in Fig. 1.

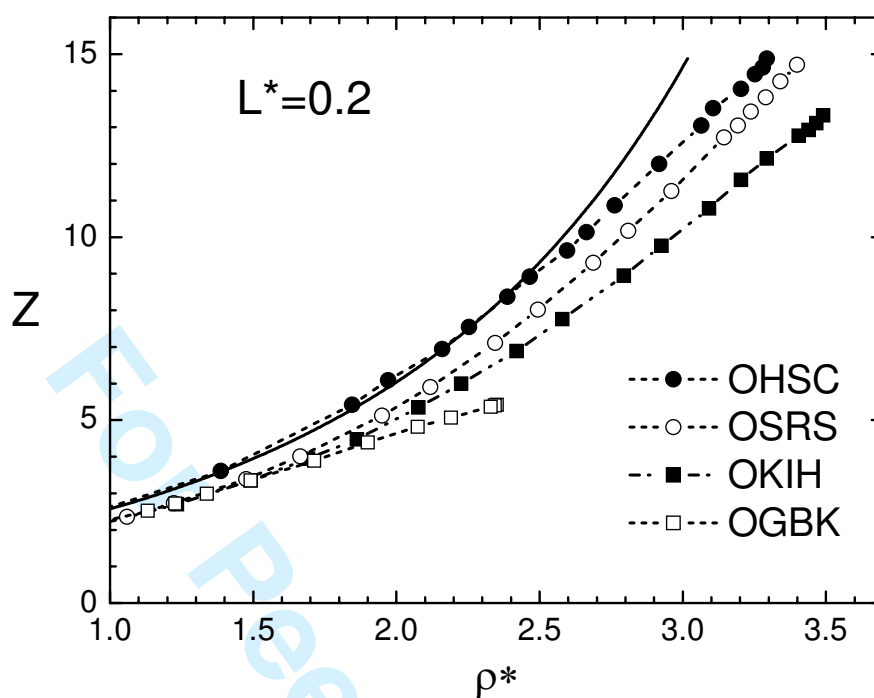


FIG. 4: Monte Carlo compressibility factor $Z=P^*/\rho^*$ versus reduced density $\rho^*=\rho D^3$ representation of the isotropic phase equations of state of the hard and soft discotic potential models considered in this work with $L^*=0.2$. The theoretical OHSC EOS from ref. [24] is also included for reference (solid line).

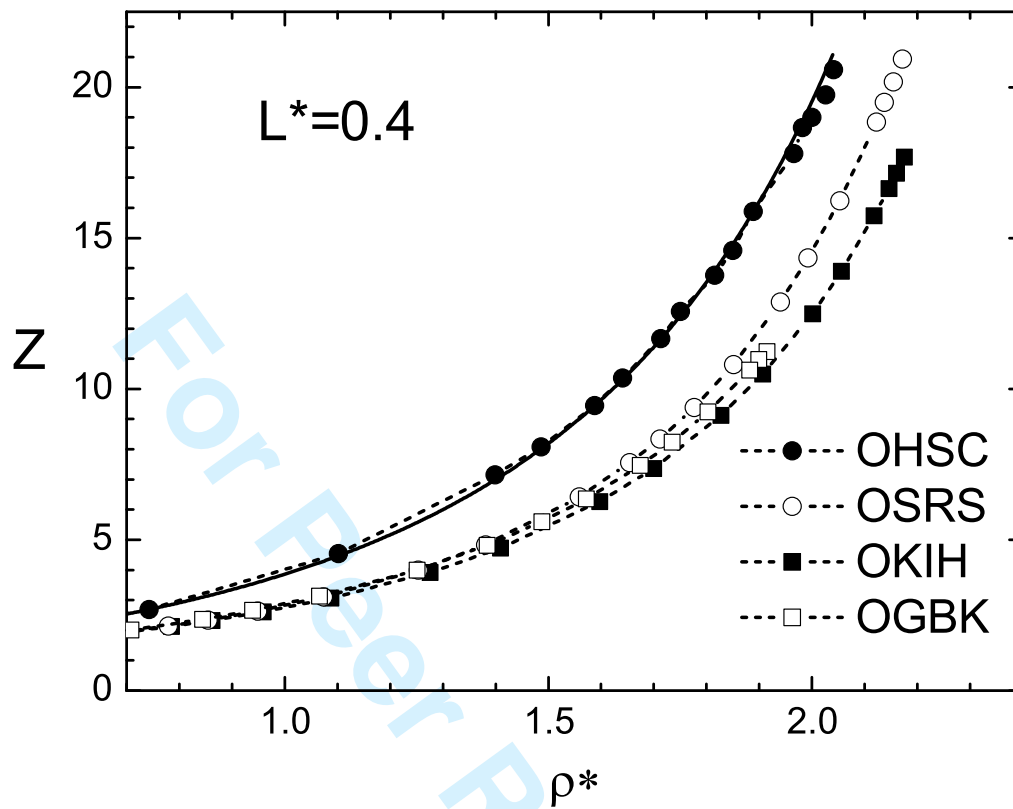


FIG. 5: Same as Fig. 4 for the hard and soft discotic potential models with $L^*=0.4$. The theoretical OHSC EOS from ref. [24] is also included for reference (solid line).

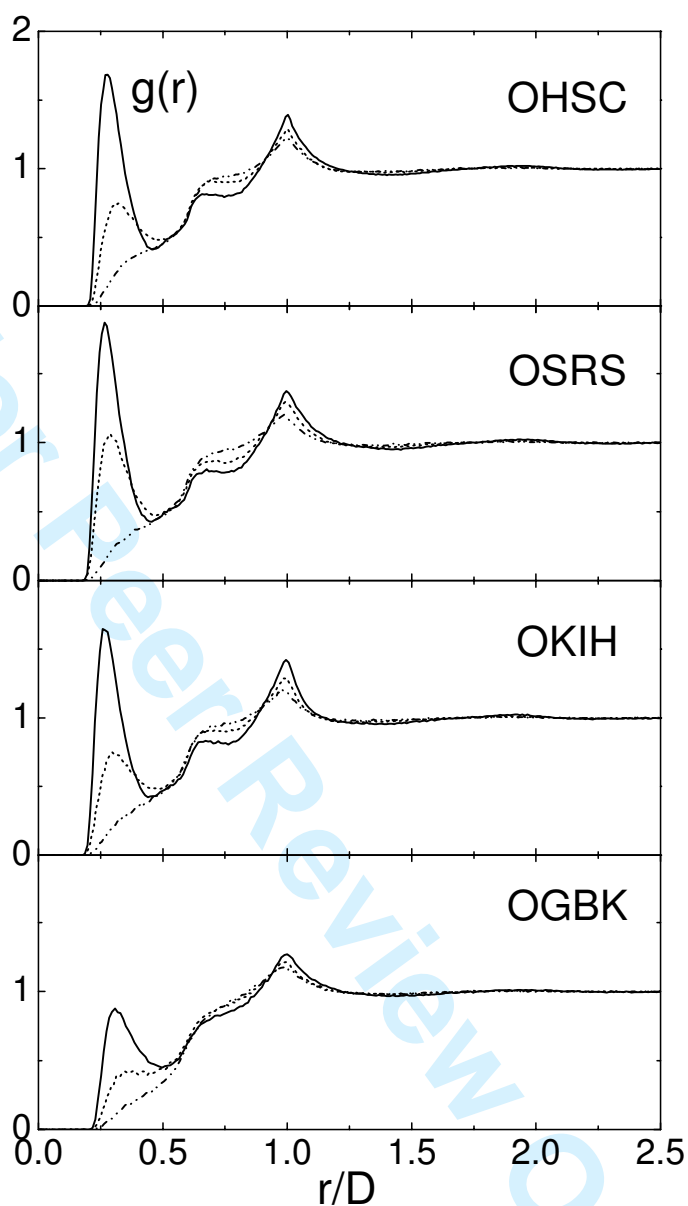


FIG. 6: Radial distribution functions, $g(r)$, for the OHSC, OSRS, OKIH and OGBK fluids with $L^*=0.2$. For each fluid, the $g(r)$ is shown for the isotropic boundary state (solid line) of the transition, and at states with densities roughly 85, and 65 percent of the boundary state density (dashed line and dot-dashed line, respectively). The pronounced peaks at $r/D \approx L^*$ are indicative of local stacking of the particles.